IYOEXPERIENCES WITH THE ORIENTATION AND CALIBRATION OF AERIAL LINEAR ARRAY CCD SENSORS

S. Kocaman, A. Gruen

ETH Zurich, Institute of Geodesy and Photogrammetry, CH-8092 Zurich, Switzerland
<skocaman><agruen>@geod.baug.ethz.ch

KEY WORDS: Calibration, Orientation, Three-Line, Scanner, Pushbroom

ABSTRACT

Solutions for the georeferencing problem of the airborne Linear Array CCD imagery employ both the existing and new photogrammetric algorithms. Due to their fairly new and complex geometry, the photogrammetric triangulation and calibration procedures for these sensors require redefinition of the existing algorithms and new software developments. A modified bundle adjustment model with the possibility of use of three different trajectory models and a specially defined set of calibration parameters have been developed at the Institute of Geodesy and Photogrammetry, ETH Zurich and implemented in our in-house software, called TLS-LAB (**T**hree-**L**ine-**S**canner **L**inear **A**rray **B**undle). A number of statistical procedures for gross error detection, determinability and significance analysis of unknown parameters, and accuracy assessment, in terms of theoretical and empirical accuracy, are connected to the adjustment model and implemented in the TLS software.

The main focus of this paper is the orientation and calibration of aerial Linear Array CCD sensors. We have tested our methods and algorithms using the imagery of a number of aerial Linear Array CCD sensors, in particular Three-Line-Scanners, for over 6 years. Several testfield datasets, which were acquired using the ADS40 sensor of the Leica Geosystems, Heerbrugg, and two out of four different engineering models of the STARIMAGER sensor, developed by former Starlabo Corp., Tokyo, have been processed within this framework. The results obtained from a selection of these testfield datasets are summarized in this paper. Several aspects related to the block geometry, data quality, and used algorithms are considered for evaluation.

1 INTRODUCTION

The introduction of digital line sensors into the field of aerial photogrammetry has provided a challenging research area for photogrammetrists due to its fairly new sensor geometry and wide-range of spectral data availability. Cameras based on Linear Array CCD sensors like the Wide Angle Airborne Camera WAAC (Boerner et al., 1997), the High Resolution Stereo Camera HRSC (Wewel et al., 1999), the Digital Photogrammetric Assembly DPA (Haala et al., 1998) were the first digital systems being used for airborne applications. The first commercial line scanner Airborne Digital Sensor ADS40 was developed by LH Systems jointly with DLR (Reulke et al., 2000, Sandau et al., 2000). In the year 2000, Starlabo Corporation, Tokyo designed the airborne Three-Line-Scanner (TLS) system, jointly with the Institute of Industrial Science, University of Tokyo (Murai and Matsumoto, 2000). The system was lately called STARIMAGER.

A modified bundle adjustment algorithm has been developed by Gruen and Zhang (2003) for triangulation of the TLS imagery. Three different types of trajectory models have been addressed in this study: (a) Direct georeferencing model with stochastic exterior orientations (DGR), (b) Piecewise Polynomials with kinematic model up to second order and stochastic first and second order constraints (PPM) and (c) Lagrange Polynomials with variable orientation fixes (LIM). These models are used for the improvement of the exterior orientation parameters, which are measured by the in-flight GPS and the INS systems. A number of ground control points are needed for this approach in order to achieve high accuracies.

Later on, the self-calibration capability was added to the sensor model using 18 additional parameters (APs) to model the systematic errors of the camera (Kocaman, 2003, and Kocaman et al., 2006). The APs can be categorized as (a) lens-based

parameters (such as camera constant, radial symmetric lens distortion, etc.) and (b) CCD-line based parameters (such as CCD line inclination, displacement of the CCD line centres from the principal point, etc.). Thus, our self-calibration model is flexible and can be extended for applications to other types of aerial and satellite sensors having multiple lenses and different numbers of Linear Array CCDs. As an example, two of our trajectory models and the self-calibration model are modified for another project currently running at our Group, the orientation and calibration of the PRISM sensor, onboard of the Japanese ALOS satellite (www.photogrammetry.ethz.ch).

The main aim of this paper is to provide an overview of our experiences with the triangulation and self-calibration of the aerial Linear Array CCD sensors. The following aspects related to the block geometry, data quality, and used algorithms are considered for evaluation:

- Flight configurations (flying height, strip distribution, overlap)
- GCP distribution (number, homogeneity) and measurement quality (both in image and object space)
- Quality of the given data obtained from external measurement devices, mainly the GPS and INS data
- Handling of stochastical model elements in the adjustment
- Trajectory model (the DGR, the LIM, and the PPM when available) with different options (i.e. number of orientation fixes or trajectory segments)
- Effect of additional parameters on the theoretical and empirical accuracy results and statistical analysis of parameter determinability

The image datasets of the ADS40 and the STARIMAGER sensors acquired over several testfields are used in our tests. The methods of triangulation, self-calibration, and accuracy assessment are briefly explained in section 2. The descriptions

of the sensors and test datasets are provided in section 3, and the results are analyzed respectively.

2   METHODOLOGY

Our methods of triangulation of Linear Array CCD sensors can employ three different trajectory models. Self-calibration capability is added to each trajectory model, with a set of statistical analysis tools.

2.1   Trajectory Models

Three different trajectory models are developed in the TLS-LAB software. Here we give an overview. For details we refer to Gruen and Zhang (2003).

The **DGR** is the simplest of the all three models. The image trajectory is modeled as a whole. 9 systematic error (3 positional shifts, 3 attitude shifts and 3 attitude drifts) parameters are estimated per trajectory. Observation equations used in the DGR model are:

$$
\begin{aligned}
v_c &= Ax_{off} + B_s x_s + B_d x_d + Cx_g & - l_c \,; & \quad P_c \\
v_{off} &= x_{off} & - l_{off} \,; & \quad P_{off} \\
v_s &= \qquad\quad x_s & - l_s \,; & \quad P_s \\
v_d &= \qquad\qquad\quad x_d & - l_d \,; & \quad P_d \\
v_g &= \qquad\qquad\qquad\quad x_g & - l_g \,; & \quad P_g
\end{aligned}
$$

The first equation of this system is the linearized observation equation of the collinearity condition. x_{off} is the unknown positional offset vector; x_s and x_d are the unknown INS shift and drift terms respectively; x_g is the ground coordinates vector; A, B_s, B_d and C are the corresponding design matrices; v, l and P are the respective residual and discrepancy vectors and weight matrices.

With the **LIM**, the exterior orientation parameters are determined in the so-called orientation fixes, which are introduced at certain time intervals. Between the orientation fixes, the exterior orientation parameters of an arbitrary scan line are interpolated using the Lagrange polynomials. This method has been developed by Ebner et al. (1992) for the orientation of MOMS images, and modified by Gruen and Zhang (2003) according to the TLS sensor model with the provision of auxiliary position/attitude data generated by the GPS/INS system. The observation equations used for bundle adjustment with the LIM model are:

$$
\begin{aligned}
v_c &= Ax_{off} + Bx_s + Cx_g & - l_c \,; & \quad P_c \\
v_{off} &= x_{off} & - l_{off} \,; & \quad P_{off} \\
v_s &= \qquad\quad x_s & - l_s \,; & \quad P_s \\
v_g &= \qquad\qquad\quad x_g & - l_g \,; & \quad P_g
\end{aligned}
$$

The first equation of this system is again the linearized observation equation of the collinearity condition, but now related to the LIM concept. x_{off} is the unknown positional offset vector; x_s is the unknown INS shift term; x_g is the ground coordinates vector; A, B and C are the corresponding design matrices; v, l and P are the respective residual and discrepancy vectors and weight matrices.

The **PPM** has been often used to model the satellite platform trajectory with respect to time (Lee et al. 2000). In this model, the values of the exterior orientation parameters are written as polynomial functions of time. The bundle adjustment determines the polynomial coefficients instead of the exterior orientation parameters themselves. Due to the instability of the high-order polynomial models, the PPM is used in piecewise polynomial fashion, in which the full complex trajectory is

divided into sections, with each section having its own set of low-order polynomials. Continuity constraints on the orientation parameters at the section boundaries ensure that the calculated positions and attitudes are continuous across the boundaries. The PPM is preferred more often in the satellite image orientation, since there the trajectories are smoother in comparison to the aerial Linear Array CCD applications. The PPM has been tested by Gruen and Zhang (2003) only in the GSI area, Japan. It has not been used in the later tests of the TLS sensors. The overall estimation model of the PPM is:

$$
\begin{aligned}
v_c &= Ax_{dis} + Bx_s + Cx_g & - l_c \,; & \quad P_c \\
v_{A1} &= A_1 x_{dis} & - l_{A1}; & \quad P_{A1} \\
v_{A2} &= A_2 x_{dis} & - l_{A2}; & \quad P_{A2} \\
v_{B1} &= \qquad\quad B_1 x_s & - l_{B1}; & \quad P_{B1} \\
v_{B2} &= \qquad\quad B_2 x_s & - l_{B2}; & \quad P_{B2} \\
v_g &= \qquad\qquad\quad x_g & - l_g \,; & \quad P_g
\end{aligned}
$$

where the first equation of this system is the linearized observation equation of the collinearity condition and the following four equations are derived from the two kind of constraints; x_{dis} contains the unknown translational displacement correction terms (ΔX, ΔY, ΔZ) for all spline sections; x_s is the unknown attitude translational error vector ($\Delta\omega$, $\Delta\varphi$, $\Delta\kappa$) for all spline sections; x_g is the ground coordinate vector; A, A_1, A_2, B, B_1, B_2, and C are the corresponding design matrices; v, l and P are the respective residual and discrepancy vectors and weight matrices. Through this consequent weighting scheme much flexibility is obtained with respect to the modeling of different trajectory conditions.

2.2   Self-calibration model

The physical structure of the TLS camera is considered in the self-calibration model. A total of 18 additional parameters (APs) have been identified, implemented, and tested. The AP set consists of lens-related and CCD line-based parameters. The lens-related parameters are:
   - Δc: Systematic error in the focal length of the camera lens.
   - *Lens Distortion Parameters:* Radial symmetric lens distortion (k_1, k_2, k_3) and decentering distortion (p_1, p_2) models of Brown (1971).

The Linear Array CCD related parameters are:
   - Δx_{pb}, Δx_{pn}, Δx_{pf}: Displacements of the line centers of the three Linear Array CCDs from the principle point (PP) of the camera lens, defined in the flight direction.
   - Δy_{pb}, Δy_{pn}, Δy_{pf}: Displacements of the line centers of the three Linear Array CCDs from the principle point (PP) of the camera lens, defined across the flight direction.
   - s_{yb}, s_{yn}, s_{yf}: Each line is subject to one scale factor, providing for the possibility of affine deformations of the individual images.
   - $\Delta\theta_b$, $\Delta\theta_n$, $\Delta\theta_f$: The $\Delta\theta$ parameters represent the systematic errors of the inclination angle between each CCD line and the (y) axis of the camera coordinate system.

The functional model of self-calibration is described in Kocaman et al. (2006).

The self-calibration algorithm presented here aims to determine the optimal set of APs for the optimal estimation of the object space coordinates of the measured image points. The adjustment procedure starts with the full parameter set and eliminates undeterminable parameters automatically in an iterative approach. The APs are introduced as free unknowns into the system. The major problem for parameter elimination is the finding of robust criteria for rejection of undeterminable

parameters. A stepwise parameter elimination algorithm proposed by Gruen (1985) is used here. The algorithm includes:

- Determinability check by analyzing the diagonal elements of the factorized normal matrix during Cholesky decomposition
- Analysis of the negative effect of each AP on the object space coordinates of the points by using the trace check algorithm of the covariance matrix
- Correlation analysis between the APs and the exterior orientation (EO) parameters, and also between the APs and the points' object space coordinates (an additional parameter having a correlation coefficient > 0.9 with the EO parameters or object space coordinates is deleted from the system)
- Statistical significance tests under *Student's t distribution* ($t_\alpha = 0.05$) for the individual analysis of the APs; and use of *Fisher distribution* ($F_\alpha = 0.05$) for the analysis of subsets of APs. Four groups of APs, which consist of (Δx_{pb}, Δx_{pn}, Δx_{pf}), (Δy_{pb}, Δy_{pn}, Δy_{pf}), (s_{yb}, s_{yn}, s_{yf}), ($\Delta\theta_b$, $\Delta\theta_n$, $\Delta\theta_f$), are tested with the F-distribution due to strong correlations between the parameters of the same group.

2.3 Accuracy Assessment Parameters

The internal and external accuracies of bundle adjustment are assessed using different parameters. The internal accuracy is expressed in terms of theoretical accuracy (precision) parameters. The covariance matrix is defined as a measure of precision of the solution $\hat{x}$ in the bundle block adjustment (Gruen, 1982). The a posteriori sigma naught value and the elements of the covariance matrix Q_{xx} are used to compute the individual standard deviations of the object points. The a posteriori sigma naught is computed using:

$$\hat{\sigma}_0^2 = \frac{1}{r}(M\hat{x}-l)^T P(M\hat{x}-l)$$

where l is the observations vector, M is the coefficients matrix, $\hat{x}$ is the solution vector of the unknown parameters, P is the weight coefficient matrix, and r is the adjustment redundancy. The standard deviations of the object point coordinates are:

$$\hat{\sigma}_{X_i} = \hat{\sigma}_0\sqrt{q_{X_iX_i}} \qquad \hat{\sigma}_{Y_i} = \hat{\sigma}_0\sqrt{q_{Y_iY_i}} \qquad \hat{\sigma}_{Z_i} = \hat{\sigma}_0\sqrt{q_{Z_iZ_i}}$$

where $q_{X_iX_i}$, $q_{Y_iY_i}$, $q_{Z_iZ_i}$, are diagonal elements of the covariance matrix Q_{xx}.

The mean standard deviations of the adjusted ground point coordinates are used as theoretical accuracy parameters and computed via the law of error propagation:

$$\hat{\sigma}_X = \sqrt{\frac{\sum_{i=1}^{n_X}\hat{\sigma}_{X_i}^2}{n_X}} \qquad \hat{\sigma}_Y = \sqrt{\frac{\sum_{i=1}^{n_Y}\hat{\sigma}_{Y_i}^2}{n_Y}} \qquad \hat{\sigma}_Z = \sqrt{\frac{\sum_{i=1}^{n_Z}\hat{\sigma}_{Z_i}^2}{n_Z}}$$

with n_X, n_Y, n_Z … number of point coordinates used for the computation, and $\hat{\sigma}_{X_i}$, $\hat{\sigma}_{Y_i}$, $\hat{\sigma}_{Z_i}$ … average standard deviations of the X,Y,Z coordinates obtained from the covariance matrix. These parameters are computed and evaluated separately for control, check and tie points.

The absolute (external) accuracy is evaluated by using reference data. The differences between the given and estimated coordinates of check points (CP) are calculated to obtain the residuals as:

$$\Delta\hat{X}_i = \hat{X}_i - X_i^r$$
$$\Delta\hat{Y}_i = \hat{Y}_i - Y_i^r$$
$$\Delta\hat{Z}_i = \hat{Z}_i - Z_i^r$$

where $\hat{X}_i$, $\hat{Y}_i$ $\hat{Z}_i$ are the estimated ground coordinates of a CP i, and X_i^r, Y_i^r Z_i^r are the reference coordinates. The *RMSE* values are computed from the residuals of CPs via:

$$\hat{\mu}_X = \sqrt{\frac{\sum_{i=1}^{n_X}\Delta\hat{X}_i^2}{n_X}} \qquad \hat{\mu}_Y = \sqrt{\frac{\sum_{i=1}^{n_Y}\Delta\hat{Y}_i^2}{n_Y}} \qquad \hat{\mu}_Z = \sqrt{\frac{\sum_{i=1}^{n_Z}\Delta\hat{Z}_i^2}{n_Z}}$$

with n_X, n_Y, n_Z … number of CP coordinates.

The theoretical and the empirical accuracies of the *X* and *Y* axes are combined and represented as one parameter set, called planimetric parameters. The formulations of the average planimetric standard deviation and the RMSE are as follows:

$$\hat{\sigma}_{XY} = \sqrt{\frac{\hat{\sigma}_{X_i}^2 + \hat{\sigma}_{Y_i}^2}{2}} \qquad\qquad \hat{\mu}_{XY} = \sqrt{\frac{\hat{\mu}_{X_i}^2 + \hat{\mu}_{Y_i}^2}{2}}$$

3 TEST RESULTS AND ANALYSIS

3.1 STARIMAGER Tests

The STARIMAGER system was developed by Starlabo Corp., Japan jointly with the Institute of Industrial Science, University of Tokyo. Four engineering models, namely SI-100, SI-250, SI-290, and SI-290N, with varying numbers of CCD lines and numbers of pixels in each, have been presented by Starlabo Corporation. Here we present the results of our methods applied to the imagery of the SI-100 and the SI-290 systems. The main parameters of the sensors are given in Table 1.

Table 1. Main parameters of the SI-100 and SI-290 sensors

Sensor/parameter	SI-100	SI-290
Focal length	60 mm	93 mm
Number of pixels per array	10 200	14 400
Pixel size	7 μm	5 μm
Number of CCD arrays	3×PAN	10 (3 directions with RGB and NIR)
Stereo view angle	21/42° *	15°, 23°, 38°, etc.

forward-nadir/forward-backward stereo view angle

3.1.1 GSI, Japan Tests

The GSI test area is covered by a strip of 650 × 2500 m². The images were acquired using the SI-100 sensor with a footprint of about 5.6 cm. 48 GCPs have been collected with GPS and measured in the images. The dataset was processed using the three trajectory models and the results were published in Gruen and Zhang (2003).

With different numbers and distributions of control points and tie points, 4.9-6.3 cm and 8.6-9.4 cm absolute accuracy in planimetry and height was achieved using the DGR model. Using the PPM or the LIM, with different numbers of segments or orientation fixes, respectively, 2.6-6.0 cm and 4.9-11.7 cm absolute accuracy in planimetry and height was attained. The LIM results were slightly better than the PPM results in these tests. Expressed in pixel size, the achieved ground point determination accuracy was 0.5-1.2 pixel in planimetry and 0.7-2.1 pixel in height. However, the given data does not represent the accuracy limit of the system, because both the image measurements and the accuracy of the GCPs did not present the state-of-the-art.

Later on, self-calibration has been applied to the dataset. However, the accuracy results did not improve significantly, probably due to high noise level in the dataset.

3.1.2 Yoriichio, Japan Tests

Two different image datasets acquired over the Yoriichio testfield with the SI-100 and SI-290 sensors were tested with the DGR and the LIM. Self-calibration was applied only to the SI-100 dataset. The main parameters of the datasets are given in Table 2.

Table 2. Main parameters of the two Yoriichio datasets

Dataset/parameter	SI-100 dataset	SI-290 dataset
Number of image strips	3	4
Flight height	600 m	1800 m
Ground sample distance	7 cm	10 cm
Total number of GCPs	61	39
Number of tie points	182	550

In the SI-290 tests, the DGR model and the LIM were used to investigate the geometrical characteristics of the SI-290 imagery. The four strips, with two parallel and two cross-strips, were used to design several test scenarios. Each scenario was tested with different numbers and distributions of control points to analyze the effect of the number of control points on the final point determination accuracy. LIM was used with gradually increasing number of orientation fixes to analyze their effect on the adjustment (Kocaman, 2005). One of the main problems of the dataset was the bad GCP image quality due to the poor signalization on the ground. For a better accuracy testing, well-signalized and well-distributed control points are crucial. These tests showed that the quality of the given trajectory data has a major effect on the accuracy results. The trajectory data used in these tests contained large systematic errors and probably a high noise level. To possibly correct these errors, the trajectory modeling of LIM is very important. In addition, with an efficient block configuration it is possible to reduce the number of control points which is necessary to reach certain accuracy level. In the LIM case, the sigma and RMSE values of the *single strip* tests performed with 6 GCPs are similar to the those of *4-strips* tests performed with 3 GCPs. *Single strip* tests have shown that a single strip has poorer geometry and a high number of control points is necessary for the system stability and trajectory modeling. With a small number of control points (<=6), it is better to use the DGR model or the LIM with a small number of orientation fixes. The best results of this dataset were obtained from the *4-strips tests* (full image block) with the LIM using 45 orientation fixes and 20 GCPs. The RMSE values are 12.6 cm (= 1.3 pixel) and 21.5 cm (= 2.2 pixels) in planimetry and in height, respectively.

In the SI-100 tests of Yoriichio, different numbers of GCPs and orientation fixes were used with and without self-calibration. The DGR model requires less control points and the accuracy remained the same with more control points. The self-calibration with the DGR model improved the sigma naught and the standard deviations only. In comparison to the DGR model, the use of a higher number of control points is necessary with the LIM. However, contrary to the DGR results, using more control points improves the accuracy significantly. When self-calibration is applied, the RMSE values and the standard deviations improved in all LIM tests. The best accuracy results in the Yoriichio testfield data were obtained with the LIM with 30 orientation fixes and with self-calibration, and using 30 GCPs. The sigma naught results in one pixel for this test configuration. The RMSE results of this test are 7 cm (= 1 pixel) and 16 cm (= 2.3 pixels) in planimetry and in height, respectively.

3.2 ADS40 Tests

Two different ADS40 sensors were used to acquire images over two different testfields. The test flight over the Vaihingen/Enz testfield was performed in summer 2004, as a joint project of Leica Geosystems and IFP Stuttgart with two different flying heights. In addition to the standard ADS40 system installation, additional GPS/inertial units were installed during the flight. The dataset was evaluated by three different groups within the framework of the EuroSDR Digital Camera Calibration project. The triangulation results of all participants are published in Cramer (2007).

The test flights over the Pavia testfield was performed by the CGR Company, Italy, in a joint project with the Geomatics Laboratory of the University of Pavia. For the detailed results of these tests, please see Kocaman et al. (2007) and Casella et al. (2007). The main parameters of the two ADS40 sensors are given in Table 3.

Table 3. Main parameters of the ADS40 sensors owned by Leica Geosystems and CGR, Italy

Sensor/parameter	Leica Geosystems	CGR, Italy
Focal length	62.7 mm	
Number of pixels/array	12 000	
Pixel size	6.5 µm	
Number of CCD arrays	10 (6×PAN, 1×RGB, 1×NIR)	10 (4×PAN, 2×Red, 2×Green, 1×Blue, 1×NIR)
Stereo view angle	B/F= 42° B/N= 14° F/N= 28° *	

B: backward, F: forward, N: nadir CCD arrays

3.2.1 Vaihingen/Enz, Germany Tests

The Vaihingen/Enz test site was established by the Institute for Photogrammetry (IFP), University of Stuttgart. The ADS40 of Leica Geosystems, Heerbrugg, was used to acquire images from two different flying heights. The data acquired in the 1500 m flight was used in our tests. The average GSD is equal to 15.6 cm. The staggered array technology was used to improve the ground resolution of the images. The GCPs and tie points were measured on the three panchromatic images (forward, nadir, backward) at the IFP, Stuttgart and provided to our group. The test dataset included a total of 6 image strips and 201 ground control points.

First, a forward intersection was applied to assess the direct georeferencing accuracy. The RMSE values are under one pixel in *X* (12 cm) and *Y* (13 cm) directions, and slightly more than one pixel in height (18 cm). This indicates already the exceptional good accuracy of the measured orientation elements.

When the bundle adjustment with the DGR model is applied, there is a certain improvement in the RMSE values especially in Y and Z directions even without using control points (Kocaman et al., 2006). In this case, the trajectory elements were introduced as weighted unknowns. The apriori standard deviations for trajectory parameters were assumed to be equal to the above mentioned RMSE (X,Y,Z) values obtained from the forward intersection process. With the use of the DGR model with 4 control points, the accuracy improved to 4.2 cm, 5.3 cm, and 6.4 cm in X, Y, and Z respectively. The same level of accuracy was obtained in case of 9 and 12 control points. When self-calibration was applied, the DGR model accuracy results improved significantly in planimetry. The theoretical sigma values and the $\hat{\sigma}_0$ obtained from the covariance matrix improved with the self-calibration as well. For this dataset, the DGR results are in general slightly better than the LIM results.

In this dataset, very accurate trajectory data was provided by the GPS/IMU system. The triangulation accuracy results with the DGR and the LIM models were about at the same level. However, the use of self-calibration improves the accuracy in terms of RMSE values in planimetry, the standard deviations of the estimated object space coordinates, and the sigma naught. According to the trace check algorithm, the additional parameters do not disturb the system's reliability.

3.2.2 Pavia, Italy Tests

The Pavia test site has been established by the Geomatics Laboratory, University of Pavia. A number of signalized and natural GCPs have been added to the site. Three different ADS40 test flights over the Pavia testfield have been performed in 2004 in a joint project with the CGR Company, Italy. 7 ADS40 strips were taken at three different flight altitudes (2000 m, 4000 m, and 6000 m). The staggered-array functionality was switched off and only one line was acquired for the backward and forward views. The triangulation and calibration approaches of the TLS-LAB and the Orima software of Leica were compared by our group and the University of Pavia group. The detailed results of the 2000 m and 4000 m image blocks are published by Casella et al. (2007) and Kocaman et al. (2007). Figure 1 shows the strip outlines of both flight datasets. The inner rectangles denote the actual processing area for triangulation. The average ground resolutions are ~20 cm and ~39 cm for the low and high flight altitudes, respectively.
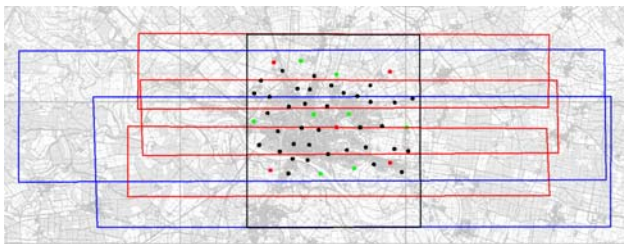
Figure 1. Structures of the 2000 m (red) and 4000 m (blue) blocks of Pavia datasets and the distributions of GCPs

Signalized GCPs with a size of 60 cm were used in this study. They were measured with a high-accuracy GPS. The red points in Figure 1 were used as control points in the tests of the 5 GCP configuration. For the 12 GCP configuration, the green points and the four red points in the corners were used. The black points were used as independent check points in all tests.

The image coordinate measurements of the control points were manually performed at the University of Pavia and provided to the ETH Zurich group. 46 and 50 signalized control points were measured on the images of the 2000 m and 4000 m flights, respectively. Tie points were extracted and measured automatically. Gross error detection procedures were performed by both Groups.

Table 4 shows the forward intersection results of the 2000 m and 4000 m flight datasets. Both datasets show systematic errors, as can be seen from the mean of the residuals. The 2000 m dataset provides a good level of accuracy, 0.5 pixels in planimetry and 3 pixels in height, even without the use of GCPs. The direct georeferencing results of the 4000 m block are worse, with 1.2 pixels in planimetry and 4.6 pixels in height.

Table 4. ETH Zurich results of direct georeferencing.

Block/parameter	2000 m			4000 m		
Component	X (m)	Y (m)	Z (m)	X (m)	Y (m)	Z (m)
RMSE	0.12	0.10	0.65	0.32	0.57	1.79
Mean	0.01	-0.01	-0.57	-0.14	0.34	-1.78
Sigma	0.10	0.10	0.22	0.15	0.18	0.39

The 2000 m flight dataset was tested using the DGR model and the LIM, with the 5 and 12 GCP configurations and both with and without self-calibration. The LIM was tested with 4 and 18 orientation fixes. The $\hat{\sigma}_0$ values of all tests ranged between 0.38-0.48 pixels. The test results without self-calibration showed large systematic errors, which however were corrected by self-calibration. The RMSE values for both models without self-calibration were between 1.0-1.3 pixels for planimetry, and 0.4-1.0 pixels for height. With self-calibration, the RMSE values were in the range of 0.2-0.5 pixels for planimetry and 0.25-0.6 pixels for height. The best results were obtained with the DGR model and self-calibration. When the DGR was compared with the LIM-18, the DGR produced more stable results. This implies that the given trajectory values were accurate and even a less complex model is sufficient for modeling the trajectory errors. The 12 GCP cases resulted in better RMSE values in comparison to the 5 GCP cases.

Regarding the 4000 m flight dataset, the DGR and the LIM were tested with the same GCP configurations (5 and 12), both with and without self-calibration. The LIM was tested with 4 and 15 orientation fixes. The $\hat{\sigma}_0$ values of all tests ranged between 0.44-0.52 pixels. The test results without self-calibration showed large systematic errors, which were corrected by self-calibration. The RMSE values obtained from the tests without self-calibration were between 0.8-1.0 pixels for planimetry, and 1.9-2.4 pixels for height. Without self-calibration, the LIM performed better in height than the DGR. Also, the use of 12 GCPs improved only the RMSE height values slightly. The self-calibration improved all RMSE values. They are in the range of 0.18-0.24 pixels for planimetry and 0.31-0.38 pixels for height. The DGR and the LIM results with self-calibration are very similar in planimetry, while in height the DGR is slightly better. The results of the 5 and 12 GCP cases are very similar in all self-calibration tests.

4 CONCLUSIONS

We have evaluated the imagery of two different airborne TLS sensors, the STARIMAGER and the ADS40, in terms of geometrical accuracy. Our methods of triangulation and self-calibration include three different trajectory models and 18 additional parameters, which have been defined according to the physical structure of the TLS sensors.

The results from three different STARIMAGER datasets, acquired over two different testfields in Japan, proved the importance of trajectory modeling in case of poor trajectory accuracy. When the given trajectory has large systematic errors and high-noise level, the final triangulation accuracy is affected and the achieved accuracy does not represent the potential of the system. The poor image and trajectory quality in all STARIMAGER datasets obstructed the efficient use of self-calibration. The results with self-calibration improved only in one dataset, the Yoriichio with SI-100, and by using a high number of GCPs with the LIM.

The stochastical model of the adjustment has a significant effect on the adjustment results, due to very high correlations between the exterior orientation unknowns. Therefore, an accurate trajectory provides a more robust solution by the possibility to use of large stochastical constraints on the unknowns. However, more investigations are still necessary on the stochastical model elements.

The images acquired with two different ADS40 sensors were tested in two different testfields. The Vaihingen/Enz block has outstanding trajectory accuracy, especially in height. The dataset could not be tested for different strip configurations due

to data access limitations. The RMSE values achieved with 4, 9, and 12 GCPs did not show significant differences. The use of self-calibration improved the RMSEs only in planimetry. Without consideration of the improvement of the GSD with the use of staggered array technology, the best RMSE values obtained in this dataset are 0.21 and 0.37 pixels in planimetry and in height, respectively. These results were obtained with the DGR and with self-calibration. The modeling of the trajectory with LIM is not necessary in this case.

In the Pavia ADS40 tests, our results are comparable to the University of Pavia results when self-calibration is used. For the 2000 m block, the best results were obtained using the DGR model with self-calibration and with 12 GCPs. In this case, the RMSE values are 4 cm and 5 cm (0.2 and 0.25 pixels) in planimetry and height, respectively. For the 4000 m block, using the DGR with 5 GCPs and with self-calibration, the RMSE values resulted in 8 cm and 12 cm (0.2 and 0.3 pixels) in planimetry and height, respectively. The use of self-calibration improved the accuracy in all cases. We should also note that the staggered array technology was switched of in the Pavia test flights.

Overall, the ADS40 tests show that;
- The APs are in general determinable under the given estimation model parameters. The trace check algorithm does not reflect high disturbances on the object point coordinates caused by the APs. Our algorithm of parameter removal is working efficiently.
- An accurate image and trajectory dataset can reach the geometric accuracy potential even with few well-defined and signalized GCPs.

All in all, there are still not enough appropriate datasets available worldwide in order to make conclusions of general value. The issue of aerial Linear Array camera accuracy performance still needs further empirical investigations, also in order to validate the different camera, trajectory and additional parameter models, and their performance under varying conditions.

5 REFERENCES

Boerner, A., Reulke, R., Scheele, M., Terzibaschian, Th., 1997. Stereo Processing of Image Data from an Airborne Three-Line CCD Scanner. The 3rd International Airborne Remote Sensing Conference and Exhibition, 7-10 July, Copenhagen, Denmark.

Brown, D.C., 1971. Close-Range Camera Calibration. Photogrammetric Engineering, 37 (8), pp. 855-866.

Casella, V., Franzini, M., Kocaman, S., Gruen, A., 2007. Triangulation and Self-calibration of the ADS40 Imagery: A Case Study over the Pavia Test Site. Proceedings of the 8th Conference on "Optical 3D Measurement Techniques", Zurich, Switzerland, 9-12 July, Vol. I, pp. 223-232

Cramer, M., 2007. The EuroSDR Performance Test for Digital Aerial Camera Systems. Proceedings of the 51st Photogrammetric Week, Stuttgart, Germany. 3-7 September, pp.89-106

Ebner, H., Kornus, W., Ohlhof, T., 1992. A Simulation Study on Point Determination for The MOMS-02/D2 Space Project Using an Extended Functional Model. IAPRS, Washington, D. C., Vol. 29, Part B4, pp. 458-464.

Gruen, A., 1982. The accuracy potential of the modern bundle block adjustment in aerial photogrammetry. Photogrammetric Engineering and Remote Sensing, Vol. 48, No. 1, pp. 45-54

Gruen, A., 1985. Data Processing Methods for Amateur Photographs. Photogrammetric Record, 11 (65), pp. 567-579.

Gruen, A., Zhang, L., 2003. Sensor Modeling for Aerial Triangulation with Three-Line-Scanner (TLS) Imagery. Journal of Photogrammetrie, Fernerkundung, Geoinformation, 2/2003, pp. 85-98.

Haala, N., Stallmann, D., Cramer, M., 1998. Calibration of Directly Measured Position and Attitude by Aerotriangulation of Three-Line Airborne Imagery. The International Archives of Photogrammetry and Remote Sensing, Budapest, Vol. 32, Part 3, pp. 23-30.

Kocaman S., 2003. Self-calibrating Triangulation with TLS Imagery. Internal Technical Report, Institute of Geodesy and Photogrammetry, ETH Zurich, 26 June.

Kocaman, S., 2005. Investigations on the Triangulation Accuracy of STARIMAGER Imagery. ASPRS 2005 Annual Conference, Baltimore, Maryland, U.S.A, 7-11 March (proceedings on CD-ROM).

Kocaman S., Zhang L., Gruen A., 2006. Self-calibrating Triangulation of Airborne Linear Array CCD Cameras. EuroCOW 2006 International Calibration and Orientation Workshop, Castelldefels, Spain, 25-27 Jan. (proceedings on CD-ROM).

Kocaman, S., Gruen A., Casella, V., Franzini, 2007. Procedings of the 28th Asian Conference on Remote Sensing, Kuala Lumpur, Malaysia, 12-16 Nov. (on CD-ROM).

Lee, C., Theiss, H. J., Bethel, J., S., Mikhail, E., M., 2000. Rigorous Mathematical Modeling of Airborne Pushbroom Imaging System. - Photogrammetric Engineering & Remote Sensing, Vol. 66, No. 4, April, pp. 385-392.

Murai, S., Matsumoto, Y., 2000. The Development of Airborne Three Line Scanner with High Accuracy INS and GPS for Analysing Car Velocity Distribution. The International Archives of Photogrammetry and Remote Sensing, Amsterdam, Vol. 33, Part B2, pp. 416-421.

Reulke, R., Franke, K-H., Fricker, P., Pomierski, T., Sandau, R., Schoenermark, M., Tornow, C., Wiest, L., 2000. Target Related Multispectral and True Color Optimization of the Color Channels of the LH Systems ADS40. The International Archives of Photogrammetry and Remote Sensing, Amsterdam, Vol. 33, Part B1, pp. 244-250.

Sandau, R., Braunecker, B., Driescher, H., Eckardt, A., Hilbert, S., Hutton, J., Kirchhofer, W., Lithopoulos, E., Reulke, R., Wicki, S., 2000. Design Principle of The LH Systems ADS40 Airborne Digital Sensor. The International Archives of Photogrammetry and Remote Sensing, Amsterdam, Vol. 33, Part B1, pp. 258-265.

Wewel, F., Scholten, F., Gwinner, K., 1999. High Resolution Stereo Camera (HRSC) – Multispectral Data Acquisition and Photogrammetric Data Processing. 4th International Airborne Remote Sensing Conference and Exhibition, Ottawa, Canada, Vol. I, pp. 263-272.